Extraction of stochastic dynamics from time series

M. Petelczyc* and J. J. Żebrowski†
Faculty of Physics, Warsaw University of Technology, Warsaw, Poland

J. M. Gac‡
Faculty of Chemical and Process Engineering, Warsaw University of Technology, Warsaw, Poland

(Received 17 June 2011; revised manuscript received 11 March 2012; published 11 July 2012)

We present a method for the reconstruction of the dynamics of processes with discrete time. The time series from such a system is described by a stochastic recurrence equation, the continuous form of which is known as the Langevin equation. The deterministic f and stochastic g components of the stochastic equation are directly extracted from the measurement data with the assumption that the noise has finite moments and has a zero mean and a unit variance. No other information about the noise distribution is needed. This is contrary to the usual Langevin description, in which the additional assumption that the noise is Gaussian (δ-correlated) distributed as necessary. We test the method using one dimensional deterministic systems (the tent and logistic maps) with Gaussian and with Gumbel noise. In addition, results for human heart rate variability are presented as an example of the application of our method to real data. The differences between cardiological cases can be observed in the properties of the deterministic part f and of the reconstructed noise distribution.

DOI: 10.1103/PhysRevE.86.011114 PACS number(s): 02.50.Ey, 02.50.Fz, 05.10.Gg, 87.10.Ed

I. INTRODUCTION

There are two main reasons for noise in real data [1]. First, as a result of the measurement process, some contamination can be superimposed on the signal in the form of measurement noise. This kind of noise does not change the dynamics of the system and is relatively easy to remove (see, e.g., [1] and references therein). We can express it as a series of random numbers added to each successive result of measurement. Another kind of noise is the so-called dynamical noise. As its name indicates, this kind of noise interacts with the dynamics of the system so that the system is perturbed by the noise at each moment in time. Measurement noise, on the other hand, only obstructs the true dynamics of the system by modifying the values measured during the evolution of the system. Dynamical noise is typically difficult to remove. Also, a small amplitude high-dimensional deterministic component of the dynamics of the system can be interpreted as dynamical noise. The most difficult are such cases for which the dynamics of the unperturbed system is nonlinear or even chaotic. Sometimes it is very difficult to distinguish the chaotic time series from a realization of a stochastic process [2]. That is the reason for a growing interest in methods for the estimation of the level of dynamical noise and, ultimately, the removal of this kind of noise from the measurement data.

There are many methods for the reduction of measurement noise, even for chaotic systems (e.g., [3,4] or the recently popular methods based on wavelet analysis, e.g., [5]). Some methods allow us to estimate the level of dynamical noise, e.g., [6,7]. However, there are very few methods for the reconstruction of a dynamical system given noisy data. One of the most promising methods is based on the Kramers-Moyal (KM) expansion (described in detail in Ref. [8] and references therein). This method assumes that the dynamical system can be described by means of the Langevin equation [9]

$$\frac{d}{dt}X(t) = D^{(1)}(X,t) + \sqrt{2D^{(2)}(X,t)}\xi(t), \tag{1}$$

where the coefficients $D^{(1)}(X,t)$ and $D^{(2)}(X,t)$ are the two first coefficients of the Kramers-Moyal expansion [10,11]. These coefficients can be obtained as the limits of the proper conditional moments which can be computed from the original results of measurement. $\xi(t)$ is δ-correlated noise with a zero mean and a unit variance. The method has been applied to many different types of time series. Initially, it was used for the analysis of the drift and diffusion coefficients in the turbulent cascade [12]. The method was successfully applied for the modeling of the human heart variability [13,14]. It seems to be a promising diagnostic tool allowing us to distinguish healthy persons from those with congestive heart failure. In Ref. [15], it was also shown that, from the dependence of the diffusion coefficient on the rescaled RR intervals (which is time between two successive R peaks in the electrocardiogram) [denoted X in Eq. (1)], new parameters of heart rate variability asymmetry can be obtained. They mirror the ability of the system regulating the heart rate to shorten or to lengthen the RR intervals.

One serious limitation of the above described method is the assumption that the noise in Eq. (1) is Gaussian (with a zero mean, standard deviation equals to one) and δ correlated. This means that the method may be applied only for systems in equilibrium [16]. We propose a KM expansion-based method of noise reconstruction in application to discrete time systems. Using conditional probability density, we develop a method to separate the deterministic term from the noise. Next, we present results of the procedure for test signals obtained from the noisy logistic and tent maps. For comparison, we considered the presence of Gaussian and Gumbel noise [17] in the test time series. Finally, we extracted the deterministic f and stochastic g components of human heart rate variability

*petelczyc_m@if.pw.edu.pl
†zebra@if.pw.edu.pl
‡j.gac@ichip.pw.edu.pl

(an RR intervals time series, recorded in a healthy male and in typical examples of atrial fibrillation, an early state of aortic valve stenosis, an advanced case of aortic valve stenosis, i.e., one with the ejection fraction less than 40%). The differences in the stochastic properties between the medical data sets analyzed are obtained, including the properties of the reconstructed noise distribution.

II. METHOD

We assume that the time series can be fully described by the stochastic recurrence equation

$$x_{n+1} = f(x_n) + g(x_n)\xi_n, \tag{2}$$

where the functions $f(x)$ and $g(x)$ are to be found. This equation is the discrete-time analog of the original continuous Langevin equation (1). ξ_n denotes a time series of the noise variable. We do not assume any form of distribution for the noise, apart for the fact that the first and the second moments of ξ exist. Let them be equal to 0 and 1, respectively. Otherwise, a simple linear transformation can be applied to ξ_n to make them fulfill the above conditions. We assume, however, that the noise has a fixed distribution, independent of n. As to the functions $f(x_n)$ and $g(x_n)$, we only assume that the last is strictly positive. If $g(x_n)$ would be equal to 0, no noise would be present in the system, of course. No further assumptions to these functions are needed.

Let us a denote $x = x_n$ and $x' = x_{n+1}$. We can then rewrite Eq. (2) in the form

$$x' = f(x) + g(x)\xi. \tag{3}$$

In this equation, we may treat x as a deterministic variable, while x' and ξ are random variables. Define $p(\xi)$ as the probability density of ξ. We can also define the conditional probability density

$$q(x' \mid x) = q(x_{n+1} = x' \mid x_n = x). \tag{4}$$

As opposed to $p(\xi)$, the approximate form of $q(x' \mid x)$ can be easily found through the analysis of the x_n series. To estimate $q(x' \mid x)$ for the given x, we first search in the time series for all the pairs $\{x_k, x_{k+1}\}$ for which $x_k = x$. In practice, this means binning the data and choosing such pairs of points $\{x_k\}$ and $\{x_{k+1}\}$ which fall into the bins of the width δ containing x and x', respectively. Let us denote the number of these pairs by N_j and also find N_i, the number of the points $\{x_k\}$ in the whole time series. The conditional probability is now given by

$$Q\left[x' \in \left(x' - \frac{\delta}{2}, x' + \frac{\delta}{2}\right) \middle| x \in \left(x - \frac{\delta}{2}, x + \frac{\delta}{2}\right)\right] = \frac{N_j}{N_i}. \tag{5}$$

The conditional probability density function $q(x' \mid x)$ can be now given by

$$q(x' \mid x) \cong \frac{N_j}{N_i \cdot \delta}. \tag{6}$$

For each bin of width δ the conditional probability Q is determined and in each the probability density is given by Eq. (6).

To determine the functions $f(x)$ and $g(x)$, we multiply (3) by $p(\xi)$ and integrate

$$\int_{-\infty}^{+\infty} x' p(\xi) d\xi = \int_{-\infty}^{+\infty} f(x) p(\xi) d\xi + \int_{-\infty}^{+\infty} g(x) \xi p(\xi) d\xi. \tag{7}$$

Since x is independent of ξ, we can rewrite (1) in the form

$$\int_{-\infty}^{+\infty} x' p(\xi) d\xi = f(x) \int_{-\infty}^{+\infty} p(\xi) d\xi + g(x) \int_{-\infty}^{+\infty} \xi p(\xi) d\xi. \tag{8}$$

On the right-hand side, the first integral is equal to 1 as an integral of the probability density function. The second integral is the mean value of ξ, equal to 0 by assumption. Thus, Eq. (2) becomes

$$f(x) = \int_{-\infty}^{+\infty} x' p(\xi) d\xi. \tag{9}$$

From elementary probability theory, if the x' is a function of ξ, the probability densities fulfill the condition

$$p(\xi \mid x) d\xi = q(x' \mid x) dx'. \tag{10}$$

On the other hand, while x and ξ are independent, we can write

$$p(\xi \mid x) = p(\xi). \tag{11}$$

From (10) and (11) together,

$$p(\xi) d\xi = q(x' \mid x) dx', \tag{12}$$

and Eq. (3) becomes

$$f(x) = \int_{-\infty}^{+\infty} x' q(x' \mid x) dx'. \tag{13}$$

To find $g(x)$, we multiply (3) by $\xi p(\xi) d\xi$ and integrate. As a result, we obtain

$$\int_{-\infty}^{+\infty} x' \xi p(\xi) d\xi = f(x) \int_{-\infty}^{+\infty} \xi p(\xi) d\xi + g(x) \int_{-\infty}^{+\infty} \xi^2 p(\xi) d\xi. \tag{14}$$

Now, the first integral on the right-hand side is equal to 0 and the second integral is equal to 1. To express the integral on the left side by x' and x, we transform Eq. (3) into

$$\xi = \frac{x' - f(x)}{g(x)} \tag{15}$$

and use Eq. (12). As a result, we obtain

$$\frac{\int_{-\infty}^{+\infty} x'^2 q(x' \mid x) dx'}{g(x)} - \frac{f(x) \int_{-\infty}^{+\infty} x' q(x' \mid x) dx'}{g(x)} = g(x). \tag{16}$$

Expression (16) is always valid as $g(x) > 0$ by assumption. By taking this into account as well as Eq. (4), we finally obtain

$$g(x) = \sqrt{\int_{-\infty}^{+\infty} x'^2 q(x' \mid x) dx' - f^2(x)}. \tag{17}$$

For some x, because of numerical errors, it may be that $\int_{-\infty}^{+\infty} x'^2 q(x' \mid x) dx' < f^2(x)$ and, as a result, Eq. (17) has

no real value. In such cases, the value of g is assumed to be less than the absolute error of its computation and is set equal to zero. The integrals in Eqs. (4) and (17) are computed numerically, e.g., by means of the trapezoidal rule.

In the next step, we have to determine the parameter δ and whether the analyzed time series is long enough to apply the method presented here. It is clear that the narrower the width of the bin δ, the more accurate the recognition of the form of the functions f and g. On the other hand, if δ is too small, too few pairs $\{x_n, x_{n+1}\}$ fulfill the relation (4). This increases the error of the method. Keeping the number of time series elements in a single bin at least 100 [18], the minimum length of the time series L should be of the order of $100 \cdot M$ where M is the total number of the bins, each of the width δ. If the smallest element of the time series is $x_{\min}$ and the maximum $x_{\max}$, we have

$$M = \frac{x_{\max} - x_{\min}}{\delta}. \tag{18}$$

That gives us the final condition that relates L and δ:

$$L \geqslant 100 \frac{x_{\max} - x_{\min}}{\delta}. \tag{19}$$

In many papers that use similar methods to ours, very long test data sets are generated to minimize the problem of poor statistics. Here, we use different examples of data set lengths, especially such that are comparable with the lengths of signals used in experiments. To avoid the problem of a large spread of the reconstructed functions at the extreme values of the argument, we limited the fitting procedure for $f(x)$ and $g(x)$ to an inner range of the argument. The details are given in the following.

III. TEST OF THE METHOD

We test the method developed in the previous section by extracting the deterministic and stochastic parts of the system from the time series. As an example, we used two different, but typical, recurrence systems to generate the artificial noisy time series. We tested the method for Gaussian and for Gumbel noise [17]. For the first test, we chose the logistic map with Gaussian white noise added and in the form

$$x_{n+1} = 2.13 x_n (1 - x_n) + (0.106 x_n + 0.02)\xi_n. \tag{20}$$

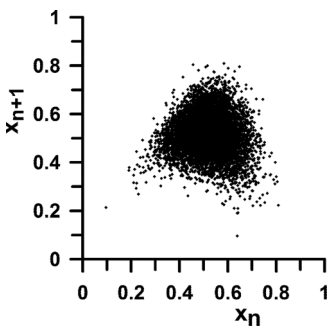

FIG. 1. Return map of the first 10^4 points generated using the recurrence equation (20) for the logistic map with multiplicative white noise.

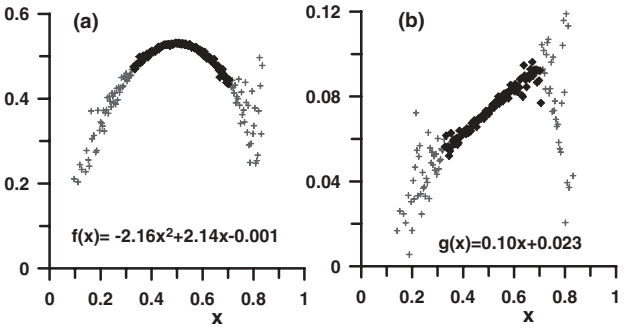

FIG. 2. Functions (a) f and (b) g determined from the data presented in Fig. 1 using the reconstruction method. The black diamonds mark the data used in the fitting procedure (see text). The functions obtained are in good agreement with those used for the generation of the data by Eq. (20).

In the above example, ξ_n is a series of white Gaussian random numbers with zero mean and a unit variance. The amplitude of the noise term is not a constant but depends on x_n. The coefficients in Eq. (20) at the noise term are arbitrary $g(x)$, but we have checked that the method works for other choices. The small constant term (0.02) was added because even a small level of noise, independent of ξ, added to the logistic equation results in a strong effect. Also, we would like to demonstrate how precise is the result of the procedure we used to extract the function $f(x)$ and $g(x)$. The map of the first 10 000 iterations of (x_n) is depicted in Fig. 1.

To obtain the function $f(x)$ and $g(x)$, we applied the method described in the previous section to the time series of the length $L = 10^5$ and $M = 200$. The plots of both extracted functions are presented in Fig. 2 as gray crosses. The function $f(x)$ can be approximately described by a quadratic equation and the function $g(x)$ is linear. These forms of the fit were assumed *a priori* as trial functions and compared to the original. A similar procedure was performed for the other systems studied here. We compared the formulas for $f(x)$ and $g(x)$ obtained from the reconstruction method with the expressions in Eq. (20). The fits are

$$f(x) = -2.022x^2 + 2.028x + 0.019, \tag{21}$$

$$g(x) = 0.083x + 0.027. \tag{22}$$

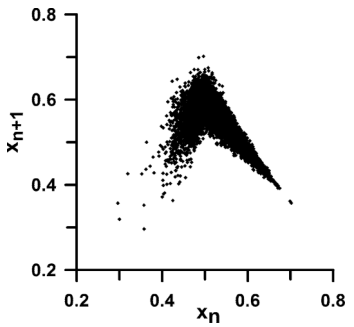

FIG. 3. Return map of the first 10^4 iterations of the recurrence equation for the tent map with multiplicative white noise [Eq. (25)].

TABLE I. The results for $f(x)$ and $g(x)$ for the tent map with $L = 10^5$.

M	$f(x)$	Pearson f	$g(x)$	Pearson g
50	$1.174x + 0.012$ and $-1.197x + 1.189$	0.994	$0.484x^2 - 0.702x + 0.258$	0.997
200	$1.179x + 0.001$ and $-1.199x + 1.197$	0.999	$0.404x^2 - 0.623x + 0.239$	0.998
400	$1.174x + 0.012$ and $-1.198x + 1.198$	0.999	$0.376x^2 - 0.592x + 0.230$	0.996
	Original $f(x)$ $f(x) = 1.2x$ for $x < 0.5$ $f(x) = 1.2(1 - x)$ for $x > 0.5$		Original $g(x)$ $g(x) = 0.45x^2 - 0.675x + 0.253$	

The coefficient of determination R^2 equals 0.87 and 0.55, respectively. Note the larger spread of the reconstructed values at both ends of the argument range. This is an effect due to the poor statistics at the external bins and results in the difference between the functions obtained and those used in the map (20). Therefore, a careful extraction of $f(x)$ and $g(x)$ from the data is critical for the method and depends on the binning. When we limited the calculation of fits to the bins in which the number of data points exceeds 100 [see Eq. (4)], we obtained a much better accuracy:

$$f(x) = -2.159x^2 + 2.139x - 0.001, \tag{23}$$

$$g(x) = 0.10x + 0.023. \tag{24}$$

Note that this limitation improved the coefficients of determinations R^2 from 0.87 to 0.97 (for f), and 0.55 to 0.91 (for g).

The accuracy of our method depends on the length of the times series L and number of bins M [see Eq. (19)]. The proper determination of the parameters L, M will be studied in detail in the following example (for the tent map with Gaussian noise):

$$\begin{aligned} x_{n+1} &= 1.2x_n + (0.45x^2 - 0.675x + 0.253)\xi_n \quad \text{for} \\ x_n &< 0.5, \\ x_{n+1} &= 1.2(1 - x_n) + (0.45x^2 - 0.675x + 0.253)\,\xi_n \quad \text{for} \\ x_n &> 0.5. \end{aligned} \tag{25}$$

The map of the first 10 000 pairs (x_n, x_{n+1}) is depicted in Fig. 3 starting from $x_0 = 0.3$. The calculations were done for $L = 10^5$, with different numbers of bins $M = 400$, 200, and 50. The functions $f(x)$ and $g(x)$ were computed for the bins for which the number of pairs was more than 100. The results of the calculations together with the Pearson coefficients are given in Table I.

A similar numerical experiment was done for a shorter time series with $L = 2 \times 10^4$ for which with $M = 400, 200, 40, 20,$ and 10. The mean and the variance of the reconstructed noise are presented in the last column of Table II.

It can be seen that computation of $f(x)$ and $g(x)$ even for shorter time series is acceptable and in good agreement with these functions used in the generation procedure. Note that the results for $g(x)$ obtained for the series with $L = 10^5$ and 2×10^4 with $M = 400$ agree relatively poorly with the original formulas, but have a high value of the Pearson coefficients. This is the effect of the indirect computation of the function $g(x)$ using Eq. (17) from the data. The accuracy of the calculation of $f(x)$ has an effect on the accuracy for $g(x)$.

The results presented in Tables I and II are in agreement with Eq. (19). Aside from keeping the number of data points in each single bin used in the calculation larger than 100, one should check the average number of x_n per bin in the calculation. As an example, in Table II for $M = 200$, the average number of points is exactly 100, while for $M = 400$, the average is 50. In the latter case, the determination of the $g(x)$ function is not accurate. Moreover, the number of bins affects also the reconstruction of the noise ξ_n using Eq. (15) (see the mean and variance in the last two columns in Table II). The larger the number of bins, the better the reconstruction of the noise. The distribution of the noise obtained from the time series with $L = 2 \times 10^4$ is the best for $M = 200$ and 400. Note, on the other hand, that for $M = 400$ the reconstruction of the functions $f(x)$ and $g(x)$ is very poor. The best quality of the extraction of $f(x)$ and $g(x)$ and of the statistical properties of the reconstructed noise ξ_n values were obtained for $M = 200$ [see Table II and Figs. 4(a) and 4(b)].

TABLE II. The results for $f(x)$, $g(x)$ for the tent map with $L = 2 \times 10^4$. Mean μ and σ^2 of the reconstructed noise distribution are shown in the last two columns.

M	$f(x)$	Pearson f	$g(x)$	Pearson g	μ	σ^2
10	$1.3x + 0.029$ and $-1.037x + 0.966$	0.825	$1.076x^2 - 1.267x + 0.393$	0.962	0.84	0.83
20	$1.116x + 0.042$ and $-1.102x + 1.12$	0.996	$0.605x^2 - 0.815x + 0.284$	0.998	0.524	0.929
40	$1.075x + 0.059$ and $-1.193x + 1.185$	0.995	$0.495x^2 - 0.713x + 0.260$	0.997	0.296	0.983
200	$1.244x - 0.021$ and $-1.205x + 1.2$	0.999	$0.40x^2 - 0.625x + 0.241$	0.981	0.064	0.996
400	$1.12x + 0.038$ and $-1.21x + 1.204$	0.999	$0.32x^2 - 0.749x + 0.276$	0.986	0.032	0.998
	Original $f(x)$ $f(x) = 1.2x$ for $x < 0.5$ $f(x) = 1.2(1 - x)$ for $x > 0.5$		Original $g(x)$ $g(x) = 0.45x^2 - 0.675x + 0.253$			

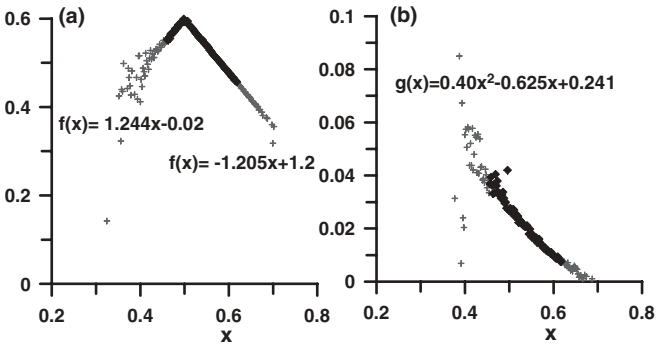

FIG. 4. Functions (a) f and (b) g determined from the data presented in Fig. 3 using the reconstruction method. The black diamonds mark the data points used in the fitting procedure (see text).

This numerical experiment shows the validity of the relation $L \geqslant 100M$ [Eq. (19)]. Each ξ_n obtained by our method is quantitatively comparable to the ξ_n used during the generation of the map. 50 consecutive values of the original time series of ξ_n are depicted in Fig. 5(a) by the black full diamonds and the reconstructed ξ_n by the empty diamonds. Figure 5(b) depicts the difference between the original values for the noise and the ξ_n obtained from our method. Note, however, that the differences depend on the quality of the reconstructed functions $f(x)$ and $g(x)$. Here, the reconstruction of ξ_n is calculated for $L = 2 \times 10^4$ and the mean and variance for reconstructed noise distribution (Table II) are acceptable even though the individual differences Δ in Fig. 5(b) are relatively large, i.e., between -0.2 and 0.2.

We will now show that the reconstruction method can be successfully applied to data with noise which has not necessarily a Gaussian distribution. As an example, we used the logistic map with Gumbel noise [17] but with the limitation of zero mean and variance equal to 1. We constructed the map in the form

$$x_{n+1} = 2.13x_n(1 - x_n) + (0.056x_n + 0.02)\xi_n. \qquad (26)$$

The first 10 000 iterations are depicted in Fig. 6. ξ_n is now Gumbel noise with the probability density function (PDF)

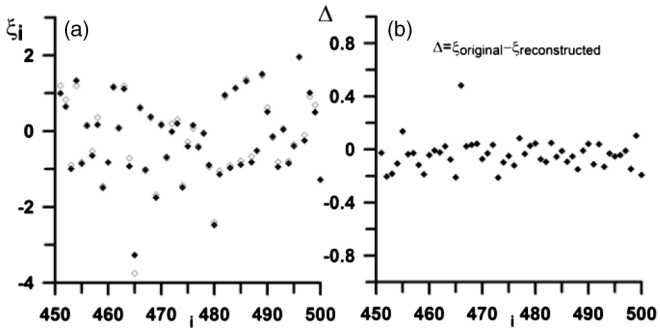

FIG. 5. (a) 50 consecutive values of the original noise ξ_n (black full diamonds) and the results of the reconstruction from the data presented in Fig. 3 (open diamonds), (b) the differences Δ between the original and the reconstructed ξ_n.

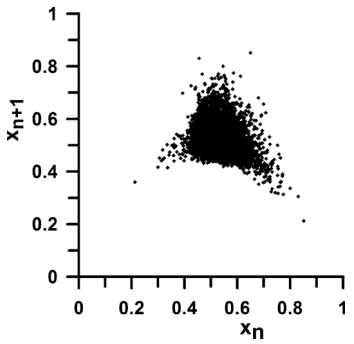

FIG. 6. Return map of the first 10^4 iterations of the recurrence equation for the logistic map with multiplicative Gumbel noise [Eq. (26)].

given by

$$P(y) = \exp\left(\frac{A-y}{B}\right)\exp\left[\exp-\left(\frac{A-y}{B}\right)\right]. \qquad (27)$$

The parameters $A, B > 0$ define the mean and the variance and were selected to obtain the properties for the moments of the distribution assumed here. $L = 10^5$ points with $M = 200$ bins were used in the calculations. The functions $f(x)$ and $g(x)$ extracted from the data are presented in Fig. 7. The black diamonds mark the bins where the number of points x_n exceeds 100 and the following fits for $f(x)$ and $g(x)$ were obtained:

$$f(x) = -2.07x^2 + 2.06x + 0.017, \qquad (28)$$

$$g(x) = 0.062x + 0.017. \qquad (29)$$

The reconstruction of the consecutive values of the noise ξ_n is presented in Fig. 8(a). A good agreement of the original values for the noise (black full diamonds) and those calculated by our method from Eq. (15) (open diamonds) was obtained. In Fig. 8(b), the difference between original values of noise and ξ_n values obtained from our method are depicted. These differences fluctuate around zero. In comparison to the results presented in Fig. 5(b), we note that the time series length was $L = 10^5$, i.e., longer than in previous cases. As a result, smaller values for Δ were obtained for this example. The parameters obtained for the distribution of the reconstructed noise were $\mu = 0.048$ and $\sigma^2 = 0.999$; the skewness was 1.087 while for the original noise data the value was 1.1395.

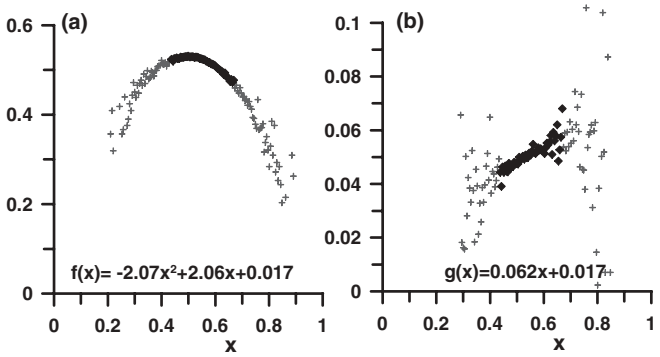

FIG. 7. Functions (a) f and (b) g determined using the reconstruction method from the data presented in Fig. 6. The black diamonds mark the data points used in the fitting procedure (see text).

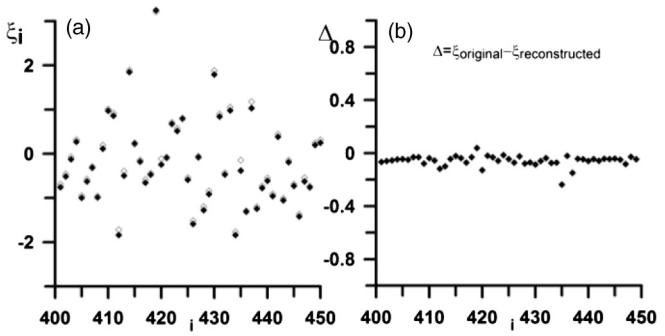

FIG. 8. (a) Example of a sequence of consecutive values of the original noise ξ_n (black full diamonds) and the corresponding reconstructed noise (open diamonds) obtained from the data presented in Fig. 6. (b) The differences Δ between the original and the reconstructed (ξ_n).

For the kurtosis, 1.98775 was obtained while for the original data it equals 2.4. The difference between the reconstructed and the original value for the kurtosis is due to its large sensitivity to outliers. Apart from this difference, the method was successfully applied to a map with Gumbel noise. Not only the deterministic and stochastic components were found, but also the reconstruction of the noise itself was performed.

IV. HEART RATE VARIABILITY ANALYSIS

Next, we applied the method to heart rate variability time series. For comparison, four different examples of heart rate variability were chosen: a healthy young male (25 years old), a male patient with atrial fibrillation (AF) (65 years old), two male patients with aortic valve stenosis, the first (ST) had an ejection fraction 71% (25 years old) and the second (LST) had an ejection fraction 40% (23 years old). In medical literature, ejection fraction is denoted %EF. Note that the data were chosen randomly (without preselection of the individual patient) from a large database of patients at the Institute of Cardiology. We analyzed 6-h-long nighttime data sets recorded between 9 p.m and 6 a.m. The heart rate variability time series, the RR intervals [19], were extracted from a 24-h Holter ECG recording using the Del Mar Reynolds system (Spacelabs) at the Institute of Cardiology (Warsaw, Poland). The data were checked manually by a cardiologist: normal beats were detected, artifacts were deleted by hand. The data were sampled at 128 Hz. No arrhythmia filtering was applied. There are a different number of points in each signal: 21801 (norm), 28831 (AF), 25701 (ST), and 18484 (LST). However, the results presented in Table III for the distribution of the noise of heart rate variability (HRV) were obtained for all examples from the first 18 470 values of ξ.

The return maps of RR intervals as well as the results of computation are presented in Figs. 9 and 10. In Fig. 9, we compare the healthy male (sinus rhythm only) and the example of atrial fibrillation. In Fig. 9(a), the "torpedo" shape of the return map typical for normals [20] can be seen: it is narrow for short RR intervals (small variance) and wider for the longer ones. The map (x_n, x_{n+1}) for AF is presented in Fig. 9(e). The occurrence of the supraventricular arrhythmia perturbs the natural dynamics of sinus heart rhythm. The functions

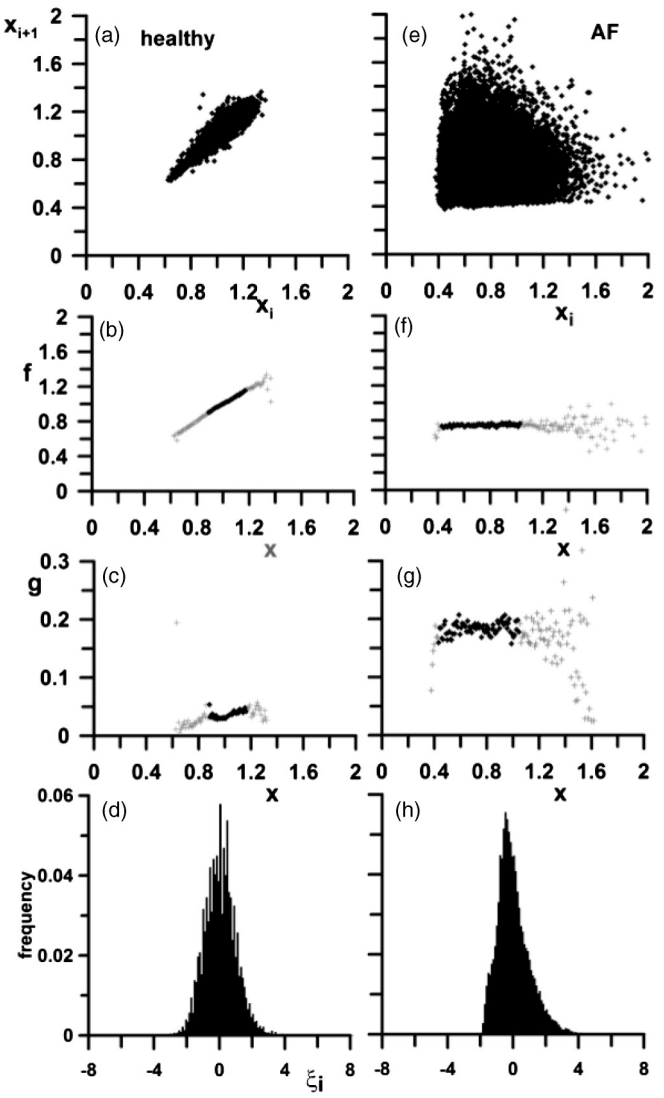

FIG. 9. Comparison of the results for heart rate variability from a healthy person (left column) with those for a patient with atrial fibrillation (right column). (a), (e) Return maps of the heart rate variability recorded at nighttime; (b), (f) the functions f determined from the time series using the reconstruction method; (c), (g) the functions g determined from the time series using the reconstruction method; (d), (g) the distribution obtained for the reconstructed noise ξ_n.

$f(x)$ for both examples are linear [Figs. 9(b) and 9(f)], but with different coefficients (see Table III). Note that $f(x)$ for AF is almost flat. What is more, the range of the function $g(x)$ is much larger for AF in comparison to the healthy case. This means that for AF the amplitude of noise is larger than for sinus rhythm. In the last row of Fig. 9, the distribution of the reconstructed noise ξ_n is given with the statistical parameters in Table III. Referring to the assumptions of our method, we obtained the means μ close to zero, and the variances σ^2 close to unity. The subtle differences are seen in the higher moments of the two distributions.

In Fig. 10, we compare two patients (of a similar age) but with different stages of aortic valve stenosis. The male with LST is at a larger risk of cardiac death than the case

TABLE III. The results for $f(x)$ extracted distribution of noise of HRV: mean, μ; variance, σ^2.

Type	$f(x)$	R^2	μ	σ^2	Skewness	Kurtosis
Healthy	$0.87x + 0.13$	0.997	0.059	0.998	0.449	2.061
AF	$0.032x + 0.721$	0.197	0.029	1.01	0.996	1.673
ST	$0.84x + 0.134$	0.997	0.033	0.967	1.331	10.321
LST	$0.864x + 0.149$	0.991	0.037	1.0	− 3.443	22.92

ST for whom the ability of the heart to pump blood is not seriously impaired. In Fig. 10(a), a torpedo shape of the return map is also visible, and no significant change of the shape compared to the normal in Fig. 9(a) is visible. The changes in the dynamics of heart rate variability due to stenosis are well visible for the case LST in Fig. 10(e). The dynamics is now completely changed: instead of a single torpedo, three "clouds" of points occur [21]. In this time series, only 1.8% of premature beats (arrhythmias) were detected so that the changes in the shape of the map indicate a different organization of sinus rhythm. The functions $f(x)$ for both examples are linear [Figs. 10(b) and 10(f)] with similar coefficients (see Table III). In Figs. 10(d) and 10(h), the distributions of the reconstructed noise are given. Their shapes differ essentially, which is consistent with the statistical parameters for these cases (Table III). The skewness for the first stenosis patient is positive, while for the LST patient it is negative. Only for this medical example, a negative skewness was obtained. The LST patient has a left asymmetric distribution of the noise. The kurtosis for the reconstructed noise for stenosis is much larger than for the healthy and for the AF case. Kurtosis for the LST patient is twice larger than for ST patient and 11 times larger than for a healthy person. To measure the sensitivity of the noise distribution potentially caused by the occurrence of the outliers, we did the following additional analysis. The calculations of the higher moments were redone for ξ values from the range ⟨mean − 3*standard deviation, mean + 3*standard deviation⟩. This range contains 99.3% of the total ξ values for the case ST, while for LST, 97.7%. We thus limited the effect of the outliers in the data on our calculation. In spite of this, we again obtained a negative skewness for LST (−0.50) and a large difference between the cases of arterial stenosis for the kurtosis (3.67 for LST versus 0.03 in ST). The medical examples are used here solely to demonstrate the application of our algorithm. A study on a much larger group of patients needs to be performed to assess the potential use of our method to medical diagnostics.

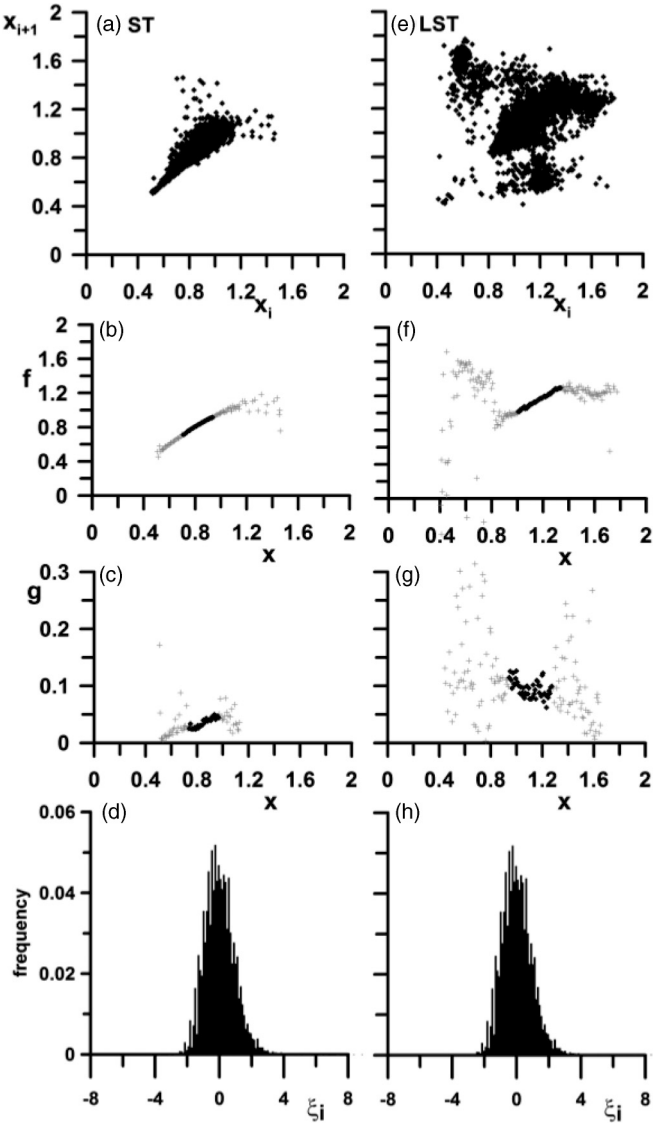

FIG. 10. Comparison of the results for heart rate variability from two patients with aortic valve stenosis: left column (ST patient) and right column (LST patient-with a low ejection fraction). (a), (e) Return maps for the heart rate variability at nighttime; (b), (f) the functions f determined from the time series using the reconstruction method; (c), (g) the functions g determined from the time series using the reconstruction method; (d), (g) the distributions obtained for the reconstructed noise ξ_n.

V. CONCLUSIONS

We present a method for the reconstruction of the dynamics of a discrete-time system from its noisy time series. The method estimates the deterministic component f and the noise term g. We showed analytically how these functions can be obtained and how they can be extracted from real data. We also discussed the practical aspects of the method given by the relation between an adequate length of the time series and the number of bins used in the computations. To ensure a good quality, we introduced limitations on the ranges of the argument in the fitting procedure used to obtain the mathematical formulas for the functions $f(x)$ and $g(x)$. We limited the analysis to such bins where the number of counts exceeds 100. Our method has the valuable advantage over

the methods based on the continuous Langevin equation. The method described here can be applied to various types of noise present in the system, not only for Gaussian noise. Note, however, that the assumption about the first two moments of its distribution is necessary: we assume that they are finite and have a zero mean and a unit variance. We tested the method on artificial time series with noise using three types of signals for the tests. These were the tent and logistic maps with multiplicative Gaussian noise with a quadratic and a linear form for the $g(x)$ function, respectively. The third test signal was obtained using the logistic map with Gumbel noise. We obtained a good agreement between the original $f(x)$ and $g(x)$ functions used to generate the time series and the series reconstructed using our method. What is more, we were able to reconstruct successfully the consecutive ξ_n for the Gaussian as well as for the Gumbel noise.

A comparison of the properties of the heart rate variability of two arterial valve stenosis patients in different stages of the advancement of the disease shows a similarity in the $f(x)$ function. The noise reconstructed for the patient with an advanced stenosis (LST) has a negative skewness and a large kurtosis. The higher moments of the noise distribution obtained for these patients indicate large differences in comparison to those of the Gaussian distribution. This seems to be in agreement with the results obtained by Hayano *et al*. [22], who showed that an increase of non-Gaussianity (measured by an index) of heart rate variability predicts cardiac mortality. On the other hand, the effect of large differences between skewness and kurtosis of the reconstructed noise for the two stenosis patients studied here could be attributed to the occurrence of outliers in the series (especially for the case of advanced stenosis LST), which affect the values of the higher moments. We therefore removed most of the outliers and found that qualitatively the results remained unchanged. In further work, we are planning to verify, using a much larger database, if the occurrence of outliers is typical for advanced stenosis. The primary aim of this paper was to demonstrate the effectiveness of our method for the reconstruction of noise from empirical data. The first results presented here may be also taken as an indication that the analysis may find application for medical diagnosis. The ability to extract the noise acting in the system is new and may be applied to study fluctuations in many different kinds of time series. Together with the analysis of the higher order Kramers-Moyal terms reported recently for heart rate variability [18], the analysis of the properties extracted noise may lead to new developments.

ACKNOWLEDGMENTS

The authors would like to thank E. Orłowska-Baranowska and R. Baranowski from the Institute of Cardiology at Warszawa for allowing us to use the medical data. The paper was supported by the Polish Ministry of Science, Grant No. 496/N-COST/2009/0, until September 2011. J.M.G. acknowledges the support of the Foundation Polish Science (Program START).

[1] M. Strumik and W. M. Macek, Phys. D (Amsterdam) **237**, 613 (2008).
[2] H. Kantz and T. Schreiber, *Nonlinear Time Series Analysis* (Cambridge University Press, Cambridge, UK, 1997).
[3] R. Cawley and G.-H. Hsu, Phys. Rev. A **46**, 3057 (1992).
[4] P. Grassberger, R. Hegger, H. Kantz, C. Schaffrath, and T. Schreiber, Chaos **3**, 127 (1993).
[5] J. Gao, H. Sultan, J. Hu, and W.-W. Tung, IEEE Signal Process. Lett. **17**, 237 (2010).
[6] K. Urbanowicz and J. A. Hołyst, Phys. Rev. E **67**, 046218 (2003).
[7] J. P. M. Heald and J. Stark, Phys. Rev. Lett. **84**, 2366 (2000).
[8] M. Siefert, A. Kittel, R. Friedrich, and J. Peinke, Europhys. Lett. **61**, 466 (2003).
[9] H. Risken, *The Fokker-Planck Equation Methods of Solutions and Applications*, Springer Series in Synergetics (Springer, Berlin, 1989).
[10] A. N. Kolmogorov, Math. Ann. **140**, 415 (1931).
[11] J. E. Moyal, Journal of the Royal Statistical Society **B11**, 150 (1949).
[12] R. Friedrich and J. Peinke, Phys. D (Amsterdam) **102**, 147 (1997).
[13] T. Kuusela, Phys. Rev E **69**, 031916 (2004).
[14] F. Ghasemi, M. Sahimi, J. Peinke, and M. Reza Rahimi Tabar, J. Biol. Phys. **32**, 117 (2006).
[15] M. Petelczyc, J. J. Żebrowski, R. Baranowski, and L. Chojnowska, Physiol. Meas. **31**, 1635 (2010).
[16] N. G. van Kampen, *Stochastic Processes in Physics and Chemistry* (North-Holland, Amsterdam, 1981).
[17] E. Bertin, Phys. Rev. Lett. **95**, 170601 (2005).
[18] M. Petelczyc, J. J. Żebrowski, and R. Baranowski, Phys. Rev. E **80**, 031127 (2009).
[19] A. L. Goldberger, L. A. N. Amaral, L. Glass, J. M. Hausdorff, P. Ch. Ivanov, R. G. Mark, J. E. Mietus, G. B. Moody, C.-K. Peng, and H. E. Stanley, Circulation **101**, e215 (2000).
[20] J. J. Żebrowski, W. Popławska, and R. Baranowski, Phys. Rev. E **50**, 4187 (1994).
[21] M. A. Woo, W. G. Stevenson, D. K. Moser, R. B. Trelease, and R. M. Harper, Am. Heart J. **123**, 704 (1992).
[22] J. Hayano, K. Kiyono, Z. R. Struzik, Y. Yamamoto, E. Watanabe, P. K. Stein, L. L. Watkins, J. A. Blumenthal, and Robert M. Carney, Front Physiol. **2**, 65 (2011).